*The American Journal of Pathology, Vol. 181, No. 3, September 2012*

*http://dx.doi.org/10.1016/j.ajpath.2012.05.031*

*Animal Models*

# Pathological Features in the *Lmna*$^{Dhe/+}$ Mutant Mouse Provide a Novel Model of Human Otitis Media and Laminopathies

Yan Zhang,*† Heping Yu,*‡ Min Xu,† Fengchan Han,*§ Cong Tian,*§ Suejin Kim,* Elisha Fredman,* Jin Zhang,† Cindy Benedict-Alderfer,* and Qing Yin Zheng*†‡§¶

*From the Departments of Otolaryngology-HNS* and Genetics,‡ and the Case Comprehensive Cancer Center,¶ Case Western Reserve University, Cleveland, Ohio; the Department of Otorhinolaryngology-HNS,† Second Hospital, Xi'an Jiaotong University School of Medicine, Xi'an, China; and the Transformative Otology and Neuroscience Center,§ Binzhou Medical University, Yantai, China*

**Genetic predisposition is recognized as an important pathogenetic factor in otitis media (OM) and associated diseases. Mutant *Lmna* mice heterozygous for the disheveled hair and ears allele (*Lmna*$^{Dbe/+}$) exhibit early-onset, profound hearing deficits and other pathological features mimicking human laminopathy associated with the *LMNA* mutation. We assessed the effects of the *Lmna*$^{Dbe/+}$ mutation on development of OM and pathological abnormalities characteristic of laminopathy. Malformation and abnormal positioning of the eustachian tube, accompanied by OM, were observed in all of the *Lmna*$^{Dbe/+}$ mice (100% penetrance) as early as postnatal day P12. Scanning electronic microscopy revealed ultrastructural damage to the cilia in middle ears that exhibited OM. Hearing assessment revealed significant hearing loss, paralleling that in human OM. Expression of NF-κB, TNF-α, and TGF-β, which correlated with inflammation and/or bony development, was up-regulated in the ears or in the peritoneal macrophages of *Lmna*$^{Dbe/+}$ mice. Rugous, disintegrative, and enlarged nuclear morphology of peritoneal macrophages and hyperphosphatemia were found in *Lmna*$^{Dbe/+}$ mutant mice. Taken together, these features resemble the pathology of human laminopathies, possibly revealing some profound pathology, beyond OM, associated with the mutation. The *Lmna*$^{Dbe/+}$ mutant mouse provides a novel model of human OM and laminopathy.** ***(Am J Pathol 2012, 181: 761–774; http://dx.doi.org/10.1016/j.ajpath.2012.05.031)***

Otitis media (OM) is a pervasive disease that involves a potential burden of hearing loss and one that in most countries leads to excessive antibiotic consumption, as well as severe complications.[1] An important susceptibility factor for OM is eustachian tube dysfunction, which can arise from developmental defects that occur as a consequence of gene mutation.

The eustachian tube and middle ear cavity differentiate from the tubotympanic recess, which develops from the endodermal lining of the first pharyngeal pouch.[2] The tympanic cavity is linked to the nasopharynx by the eustachian tube. A cartilaginous structure, the eustachian tube extends its bony ostium from the middle ear cavity to vent the middle ear and to clear and protect the middle ear from nasopharyngeal secretions. Malformation or malposition of the eustachian tube can give rise to OM, as reported in gene-mutation mouse models.[3,4]

Lamin A/C (LMNA) is a structural protein encoded by the *LMNA* gene. LMNA is an essential scaffolding component of the nuclear envelope surrounding the cell nucleus. The nuclear envelope regulates movement of molecules into and out of the nucleus. The lamin protein family, of which lamin A/C is a member, plays a role in nuclear stability, chromatin structure, and gene expression. Lamin proteins form the vertebrate nuclear lamina, a two-dimensional matrix near the inner nuclear membrane, and are highly conserved in evolution.[5] Mutations in *LMNA* cause a group of human disorders often collectively called laminopathies, which includes Hutchinson-Gilford progeria syndrome (HGPS). In a recent study,

Supported by the NIH National Institute on Deafness and Other Communication Disorders (R01-DC009246, R01-DC007392, and R21-DC005846 to Q.Y.Z.), the National Natural Science Foundation of China (30440080 to Q.Y.Z. and 30973300 to M.X.), and Shandong Province (Taishan Scholar award tshw20110575 to Q.Y.Z.).

Accepted for publication May 17, 2012.

Address reprint requests to Qing Yin Zheng, M.D., Associate Professor, Department of Otolaryngology-HNS, Case Western Reserve University, 11100 Euclid Avenue, LKS 5045, Cleveland, OH 44106, or to Min Xu, M.D., Department of Otorhinolaryngology-HNS, Second Hospital, Xi'an Jiaotong University School of Medicine, Xi'an, Shaanxi, 710004, China. E-mail: qing.zheng@case.edu or ent551205@163.com.

patients with HGPS were noted to have stiff auricular cartilage, small or absent lobules, and hypoplasia of the lateral soft-tissue portion of the external ear canal, leading to a shortened canal. Patients typically exhibit low-frequency conductive hearing loss.[6]

The *Lmna*$^{Dhe}$ mutation, first described by Odgren et al,[7] is named for the external phenotypes of sparse coat and small ears [ie, disheveled hair and ear (*Dhe*)]. This spontaneous, semidominant point mutation in the *Lmna* gene encodes an amino acid substitution, L52R, in the coiled-coil rod domain of lamin A and C proteins. The mutation is also associated with epidermal dysplasia and craniofacial defects in both heterozygotes and homozygotes; however, the homozygotes rarely survive past P10.[8]

In the present study, we found that the *Lmna*$^{Dhe/+}$ mutant mice exhibited early-onset and profound hearing defects. In characterizing the mechanisms for deafness, we further investigated the auditory system and observed OM accompanied by significant developmental defects in the eustachian tube and its adjacent basicranial structure. All of the heterozygous mutant mice developed OM, along with malformation of the eustachian tube, as early as 12 days after birth. We suggest that the *Lmna*$^{Dhe/+}$ mice provide a model for human OM associated with craniofacial defects, as well as eustachian tube malformation, and that the *Lmna*$^{Dhe}$ mutation accounts for the middle ear maturation defect. Considering these data together with our assessment of serum calcium and phosphorus abnormalities and nuclear defects of peritoneal macrophages, we inferred that *Lmna*$^{Dhe}$ mutation correlates with pathological features of laminopathy. Thus, mice expressing *Lmna*$^{Dhe}$ mutation provide a novel model for investigation of OM and laminopathy.

## Materials and Methods

### Mouse Husbandry

*Lmna*$^{Dhe/+}$ heterozygous mice were obtained from the Jackson Laboratory (Bar Harbor, ME) and were bred at the Wolstein Animal Research Facility at Case Western Reserve University. Because homozygous *Lmna*$^{Dhe/Dhe}$ pups die at approximately P10, the strain was maintained by heterozygous cross-mating. We used 78 heterozygous *Lmna*$^{Dhe/+}$ mutant mice and 68 wild-type littermate control mice, from 6 days to 8 months of age. All mice younger than 12 days were genotyped by PCR and identified by Sma1 digestion (R0141S #0831104; New England Biolabs, Ipswich, MA), as described previously.[7] All animal procedures were reviewed and approved by the Health Sciences Institutional Animal Care and Use Committee of Case Western Reserve University (protocols 2008-0174 and 2008-0156).

### Analysis of Middle Ear and Adjacent Basicranial Structure

Wild-type and *Lmna*$^{Dhe/+}$ mutant mice at 10 weeks of age were dissected immediately after $CO_2$ asphyxiation ($n = 6$ for each genotype; 3 male and 3 female mice in each group). No fixative solution was applied. Skulls were dissected and photographed under an anatomical microscope (Leica S6D; Leica Microsystems, Wetzlar, Germany). After removal of the lower jaw of the skull and dissection of the soft tissue surrounding the bullae, a short straight section of whisker from each mouse was used as a landmark and the whisker was inserted from the pharyngeal opening to the tympanic opening of the eustachian tube. The intersection angle (IA) between the eustachian tubes was measured using ImageJ software version 1.6.0_33 (32-bit) (NIH, Bethesda, MD). Dimensions of the eustachian tubes were acquired with a hand-held digital caliper (General Tools & Instruments, New York, NY) with 0.01-mm resolution.

### Tympanometry Analysis, ABR Thresholds, and DPOAE

Tympanometry measurement was performed to test the condition of the middle ear and the mobility of the tympanic membrane and the ossicles using a race car tympanometer (Maico, Berlin, Germany). The instrument was calibrated to atmospheric pressure each day, before the measurement was performed. The physical volumes of the tympanometer (1.5, 0.5, and 0.25 mL) were also calibrated.

A computer-aided evoked potential system (Intelligent Hearing Systems, Miami, FL) was used to test the mouse auditory-evoked brainstem response (ABR) thresholds and distortion product otoacoustic emissions (DPOAE), as described previously.[9] Broadband-click (8 to 16 kHz) and 8-, 16-, and 32-kHz pure-tone burst stimuli were presented to mice.

DPOAE measurement was performed using SmartOAE 4.50 USBez software (Intelligent Hearing Systems), using the Etymotic 10B+ OAE probe (Etymotic Research, Elk Grove Village, IL) fitted with a high frequency transducer (Intelligent Hearing Systems) producing two pure tones, F1 and F2. Two ranges of frequencies were tested: the low frequencies ranging from 4 to 20 kHz with the frequency per octave set at 5.0, and the higher frequencies ranging from 16 to 32 kHz with frequency per octave set at 7.0. Both ranges measured the response signals to L1 and L2 amplitudes set at 65 and 55 dB sound pressure level (SPL), respectively, with an F2/F1 ratio of 1.22. Only the data with A1 and A2 levels with the respective L1 and L2 of $\pm$15 dB SPL were considered robust; any data point falling outside of the criteria was discarded. The signal-to-noise ratios were plotted against F2.

The procedures for tympanometry measurement, ABR, and DPOAE were performed in a quiet animal room at normal room temperature with the noise level maintained below 51 dB SPL. Mice were anesthetized with 2,2,2-tribromoethanol (Avertin; 0.5 mg/g body mass) before the measurement.

### Preparation of Bullae for Histological and Immunofluorescent Staining

For histological pathology and immunohistochemical examination, mice were euthanized at ages ranging from 6

days to 8 months. Bullae were isolated from ears of wild-type mice ($n = 4$) and *Lmna*$^{Dhe/+}$ mutant mice ($n = 4$), including both the middle and inner ear. Bullae were quickly dissected after euthanization, fixed in 4% paraformaldehyde at 4°C for 24 hours, and then decalcified in 10% EDTA for age-specific periods, as follows. For 6- and 12-day-old mice, samples were decalcified for 1 and 2 days, respectively; for both 21-day-old and 8-month-old mice, samples were decalcified for 7 days. Samples were then dehydrated and embedded in paraffin blocks. The paraffin-embedded samples were sectioned serially at 5-$\mu$m thickness and mounted onto Fisher Superfrost Plus slides (Thermo Fisher Scientific, Waltham, MA).

### *H&E and Mayer's Mucicarmine Staining*

For H&E staining, a standard protocol was used.[10] In accord with the manufacturer's protocol (Electron Microscopy Sciences, Hatfield, PA), Mayer's mucicarmine staining was used to identify goblet cells in the middle ear mucosa. Sections were examined under light microscopy (DFC500; Leica Microsystems). Images were acquired at $\times 5$ to $\times 63$ magnification.

### *Scoring System for Pathology of Middle and Inner Ears*

A four-point scoring system was applied to assess the severity of pathology in middle and inner ears. Scores were assessed and analyzed simultaneously by two individuals (Y.Z. and E.F.) masked to the genotype. Discrepancies were resolved by mutual consensus. The scale was as follows: −, absence of pathology in the middle or inner ear; +, very scarce pathology; ++, prevalent pathology, but not spread throughout the entire middle or inner ear; +++, pathology infiltrating the entire middle or inner ear. The scored pathologies included middle ear effusion, inflammatory cell infiltration, tissue debris, tissue proliferation, goblet cells, and inner ear effusion. A $\chi^2$ test was used to evaluate the semiquantitative data. This method has been reported in previous OM studies.[11]

### *Scanning Electronic Microscopy*

After cardiac perfusion with 1× PBS and then with 4% paraformaldehyde, bullae were dissected from skulls of 21-day-old and 10-week-old control and *Lmna*$^{Dhe/+}$ mice ($n = 3$ mice per genotype). Samples were placed in 2.5% glutaraldehyde in cacodylic acid in 0.1 mol/L phosphate buffer (pH = 7.2) at 4°C overnight. After separation of the middle ear and inner ear, samples were postfixed with 1% osmium tetroxide diluted in 0.1 mol/L phosphate buffer. Samples were washed with distilled water three times, and then were dehydrated in serial solutions of ethanol. Each sample was subjected to $CO_2$ critical point drying, followed by sputter-coating with 60:40 gold/palladium. Samples were then viewed under a high-resolution scanning electron microscope (Helios NanoLab 650; FEI, Hillsboro, OR).

### *Peritoneal Macrophage Migration* in Vivo *and Quantification Assay*

To evaluate whether the *Lmna* mutation affected mouse macrophage migration, morphogenesis, and/or cytokine expression, primary peritoneal macrophages were cultured from 4-month-old wild-type control mice and *Lmna*$^{Dhe/+}$ mutant mice, as described below. Thioglycollate broth (60 $\mu$L/g mouse body mass) was injected intraperitoneally into six mice (three females and three males) of each genotype. The mice were euthanized 3 days later. Peritoneal macrophages were recovered by peritoneal lavage with sterile, cold (4°C) PBS, followed by red blood cell lysis. Macrophages were counted on a hemocytometer (Hausser Scientific, Horsham, PA). Cells were then distributed into sterile plates (0.5 mL cells per plate), each containing a 22 × 30-mm slide, and were incubated at 37°C under 5% $CO_2$ for 4 hours, to allow adhesion to slides for immunohistochemical staining.

### *Immunofluorescent Staining for LMNA, NF-κB, TNF-α, and TGF-β in Middle Ear Paraffin Sections and in Primary Macrophages*

Middle ear paraffin sections were deparaffinized in xylene, rehydrated in decreasing concentrations of ethanol, washed in distilled water, and incubated in trypsin working solution as described previously.[11] For macrophage staining, smears were fixed in 1.5% paraformaldehyde. Sections and smears were permeabilized in 0.2% Triton X-100, washed in PBS, and then blocked in 3% goat serum and 2% BSA. Primary antibodies of anti-NF-κB (1:200 dilution; ab7971; Abcam, Cambridge, MA), anti-TNF-α (1:200 dilution; ab9739; Abcam), anti-lamin A/C (1:300 dilution; H-110; sc-20681; Santa Cruz Biotechnology, Santa Cruz, CA), or anti-TGF-β1/2/3 (1:200 dilution; sc-7892; Santa Cruz Biotechnology) were applied and slides were incubated overnight at 4°C. After a PBS wash, sections were incubated with goat anti-rabbit conjugated to Alexa Fluor 488 (1:500 dilution; Life Technologies-Invitrogen, Carlsbad, CA) and then with propidium iodide (10 $\mu$g/mL; P1304MP; Life Technologies-Invitrogen) or DAPI (10 $\mu$g/mL; D1306; Life Technologies-Invitrogen). Sections were mounted with Vectashield mounting medium (Vector Laboratories, Burlingame, CA) and were observed under an immunofluorescence microscope (Leica DFC500). Images were acquired at magnifications of $\times 5$ to $\times 63$.

### *Semiquantitative RT-PCR*

RNA was isolated from the bullae of four mutant and four control mice at P21, using a Gibco Pure-Link micro-to-midi total RNA purification system (Life Technologies-Invitrogen, Grand Island, NY). The SuperScript III first-strand synthesis system for RT-PCR was used to synthesize cDNA. Relative mRNA expression levels for TGF-β were determined by PCR using *Gapdh* as the positive control. Primers for *Gapdh* (forward: 5′-AACTTTGGCATTGTGGAAGG-3′; reverse: 5′-GGAGA-

CAACCTGGTCCTCAG-3′) yield a 351-bp product, which spans two introns (between exons 3 to 4 and exons 4 to 5), as has been reported.[11,12] Primers for TGF-$\beta$ (forward: 5′-AGCCCGAAGCGGACTACTAT-3′; reverse: 5′-TCCACATGTTGCTCCACACT-3′) yield a 215-bp product, which spans one intron (exons 1 to 2). PCR was performed using Taq DNA polymerase (New England Biolabs) with the following amplification conditions: denaturation at 94°C for 2 minutes, followed by 31 cycles of 94°C for 30 seconds, 60°C for 40 seconds, and 72°C for 50 seconds, with a final extension step at 72°C for 5 minutes. PCR products were subjected to 2% agarose gel electrophoresis, and each yielded a single band of the predicted size. To evaluate relative gene transcription levels, a semiquantitative method was applied, using ImageJ software to normalize the TGF-$\beta$ band intensity to *Gapdh* expression. Student's *t*-test was used to analyze differences between relative gray intensity of PCR bands, as described previously.[11]

### *Measurement of Serum Phosphorus and Calcium*

Blood samples were acquired by cardiac puncture from 4-month-old wild-type and *Lmna*$^{Dhe/+}$ mutant mice ($n = 6$ mice per genotype; 3 females and 3 males). Serum was isolated and stored at −80°C. Serum calcium and phosphorus were assessed using an automated chemical analyzer (Vitros 350; Ortho Clinical Diagnostics, Johnson & Johnson, Rochester, NY) by the University of North Carolina Animal Clinical Chemistry and Gene Expression Laboratories (Chapel Hill, NC).

## *Results*

### *Abnormal Middle Ear and Adjacent Basicranial Anatomy in* Lmna$^{Dhe/+}$ *Mutants*

Morphological study and morphometric analysis at age 10 weeks revealed anatomical abnormality of the middle ear and adjacent basicranial structure in the *Lmna*$^{Dhe/+}$ mutant mice. All six dissected skulls in the mutant mice exhibited a reduced distance, and three of the six exhibited a fused gap between the roof of the nasopharynx and the palate bone, compared with wild-type mice (Figure 1). The mean intersection angle between the bilateral eustachian tube in wild-type mice was 81.89 degrees, compared with 110.48 degrees in mutant mice (Figure 1, A–C). The mean length of the bony part of the eustachian tube in wild-type mice was 1.21 mm, compared with 0.93 mm in mutant mice. The mean width of the bony part of the eustachian tube was 1.12 mm, compared with 1.82 mm in mutant mice (Figure 1, D–F). The length/width ratio was 1.08 in wild-type mice, compared with 0.52 in mutant mice (Figure 1F), which further explains the shape abnormality of the eustachian tube. Within each group, there were no statistically significant differences in measurements between males and females (data not shown). Between the mutant and wild-type groups, however, all of the measurements indicated statistically significant differ-

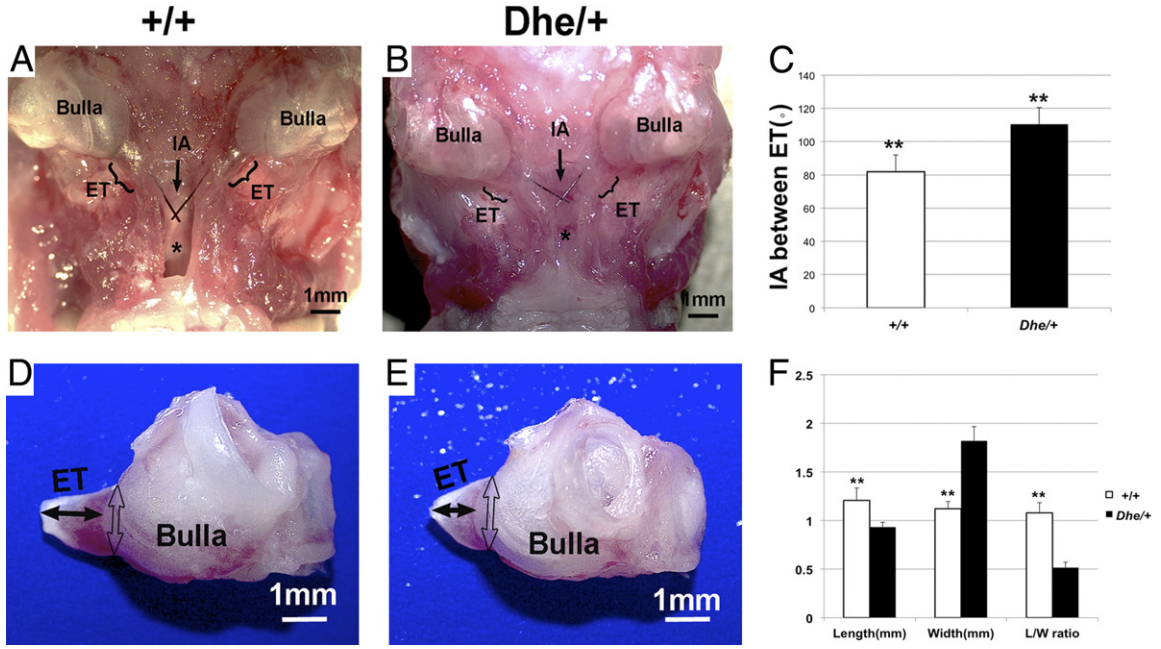


**Figure 1.** Morphological abnormality of 10-week-old *Lmna*$^{Dhe/+}$ mutant mice (*Dhe*/+) and morphometric analysis, compared with wild-type mice (++). **A** and **B:** Ventral view of the middle ear and adjacent basicranial structure in wild-type and mutant mice. Note that the roof of the nasopharynx (**asterisk**) appears abnormal in the mutant mice, compared with wild-type mice. There is barely a gap between the tissue of the nasopharynx and the palate in the mutant mice, and the roof of the nasopharynx is nearly fused to the palate bone. An **arrow** points to the intersection angle between the bilateral eustachian tube (ET); **brackets** indicate the position and length of the ET. **C:** Quantification of mean intersection angle (IA) reflects the significantly greater angulation in mutant mice, compared with wild-type mice. $n = 6$. **D** and **E:** Morphology of isolated bullae with ET. Bullae of mutant mice are smaller than those of wild-type mice. The mean length of the bony part of the ET (**solid double-ended arrows**) in the wild-type mice is greater than that of the mutant mice, whereas the ET width of mutant mice is greater (**open double-ended arrows**) than that of the wild-type mice. The mutant mice have a lower length/width (L/W) ratio than do the wild-type mice. **F:** Quantification of length and width measurements. $^{**}P < 0.01$, $n = 12$. Data are expressed as means ± SEM. Scale bar = 1 mm.

ences ($P < 0.05$). Thus, clear alterations of the intersection angle accompanied by dilated anamorphic eustachian tubes in *Lmna*$^{Dhe/+}$ mutant mice produce a morphology that mimics the conditions in humans that cause predisposition for OM.

## *Tympanometry Assessment Reveals Possible Structural Alteration in the Ears of* Lmna$^{Dhe/+}$ *Mice*

Ear function was assessed by tympanometry in mice ranging in age from 3 weeks to 8 months. No statistically significant difference was detected between the left and right ears. Mean volume (*V*) of *Lmna*$^{Dhe/+}$ mutant mice was lower than that of wild-type mice at age 3 weeks, but there was no significant difference at other ages. Mean values and standard deviations were calculated for each parameter (Table 1); tympanogram results are presented for comparison (Figure 2, A–D). The tympanometric values of compliance (*C*) were significantly lower at all time points in *Lmna*$^{Dhe/+}$ mutant mice, compared with littermate controls. Pressure (*P*) of the middle ear was measured as a significantly more negative value in *Lmna*$^{Dhe/+}$ mice, compared with the control mice. Mean gradient values (*G*) were higher in *Lmna*$^{Dhe/+}$ mice at the age of 1 month, and the difference was statistically significant. With the different stages of OM progression, gradient values may vary. Gradient values are correlated with human OM, and both adult patients with OM and healthy children have a wider range of gradient. Scanning tympanograms from 5-month-old wild-type were representative of the normal A type curve (Figure 2E), and those of mutant mice were representative of the abnormal C type curve (Figure 2F), which resembles the C curve typical in human OM. Anatomical images under otoscopy of the ears that had tympanograms consistent with OM in *Lmna*$^{Dhe/+}$ mutant mice (Figure 2H) provided further evidence of OM, in contrast to the normal anatomy in control mice (Figure 2G). Tympanic membrane adherence and hydrotympanum typical of OM were detected by otoscopy in mutants.

## *Time-Course ABR Thresholds and DPOAE*

ABR thresholds from day P16 to 4 months of age were consistently elevated in *Lmna*$^{Dhe/+}$ mutant mice, compared with the wild type (Figure 3). Mean values for ABR threshold above 55 (for click stimuli), 40 (for 8 kHz), 35 (for 16 kHz), and 60 (for 32 kHz) dB SPL indicate hearing impairment.[13] All of the *Lmna*$^{Dhe/+}$ mutant mice met the criteria for hearing loss at the lower stimulus frequencies, click and 8 kHz (Figure 3, A and B). From P30, *Lmna*$^{Dhe/+}$ mutant mice began to show a fluctuant hearing impairment at the 16 kHz stimulus frequency (Figure 3C) and a clear tendency toward elevation at the higher stimulus frequency of 32 kHz (Figure 3D). These results demonstrated that the phenotype of hearing impairment began at lower stimulus frequencies (click and 8 kHz), and with age began to affect higher stimulus frequencies (16 and 32 kHz). At 3 months of age, *Lmna*$^{Dhe/+}$ mice had DPOAE 10 to 43.5 dB lower than those of wild-type mice at frequencies from 7.6 to 23 kHz (Figure 3E).

## *Histological Detection of OM and Developmental Malformation of the Eustachian Tube*

Histological pathology was assessed at various stages to track the occurrence of OM inflammation and of eustachian tube developmental malformation in *Lmna*$^{Dhe/+}$ mutant mice, compared with littermate control wild-type mice (Figure 4). The middle ear was undeveloped at P6. No significant developmental disparity between wild-type and mutant or occurrence of middle ear inflammation were detected (Figure 4, A–F). At 12 days, with middle ear cavitation still progressing, significant dysplasia occurred with dilation of the eustachian tube. Cells of the acute inflammatory response began to perfuse the MEC of *Lmna*$^{Dhe/+}$ mice, to infiltrate the mesenchymal cells and to block the eustachian tube (Figure 4, K and L). The tympanic membrane was undeveloped at this stage (Figure 4, J–L). At weaning age of 21 days, the trend of inflammation continued and malformation of the eustachian tube was irreversible in *Lmna*$^{Dhe/+}$ mutant mice

**Table 1.** Tympanometry Measurements over a Time Course in Wild-Type and *Lmna*$^{Dbe/+}$ Mutant Mice

| Age and genotype | V (mL) | C (mL) | P (daPa × 1000) | G (daPa × 1000) |
|---|---|---|---|---|
| 3 weeks | | | | |
| Wild-type | 0.251 ± 0.047 | 0.49 ± 0.045$^{\dagger}$ | −0.014 ± 0.018$^{\dagger}$ | 0.142 ± 0.042 |
| Mutant | 0.261 ± 0.041 | 0.26 ± 0.108$^{\dagger}$ | −0.063 ± 0.018$^{\dagger}$ | 0.135 ± 0.042 |
| 1 month | | | | |
| Wild-type | 0.322 ± 0.016$^{\dagger}$ | 0.71 ± 0.152* | −0.025 ± 0.011* | 0.098 ± 0.031$^{\dagger}$ |
| Mutant | 0.252 ± 0.016$^{\dagger}$ | 0.59 ± 0.140* | −0.034 ± 0.022* | 0.135 ± 0.033$^{\dagger}$ |
| 5 months | | | | |
| Wild-type | 0.341 ± 0.048 | 0.74 ± 0.143$^{\dagger}$ | −0.021 ± 0.017 | 0.132 ± 0.020 |
| Mutant | 0.331 ± 0.037 | 0.45 ± 0.134$^{\dagger}$ | −0.041 ± 0.022* | 0.141 ± 0.031 |
| 8 months | | | | |
| Wild-type | 0.342 ± 0.052 | 0.80 ± 0.173$^{\dagger}$ | −0.015 ± 0.018$^{\dagger}$ | 0.124 ± 0.035 |
| Mutant | 0.334 ± 0.046 | 0.49 ± 0.119$^{\dagger}$ | −0.053 ± 0.027$^{\dagger}$ | 0.151 ± 0.042 |

Data are presented as means ± SD. $n \geq 6$ mice at each age and each genotype.
*$P < 0.05$, $^{\dagger}P < 0.01$.
C, compliance; G, pressure gradient; P, pressure in middle ear; V, ear volume.

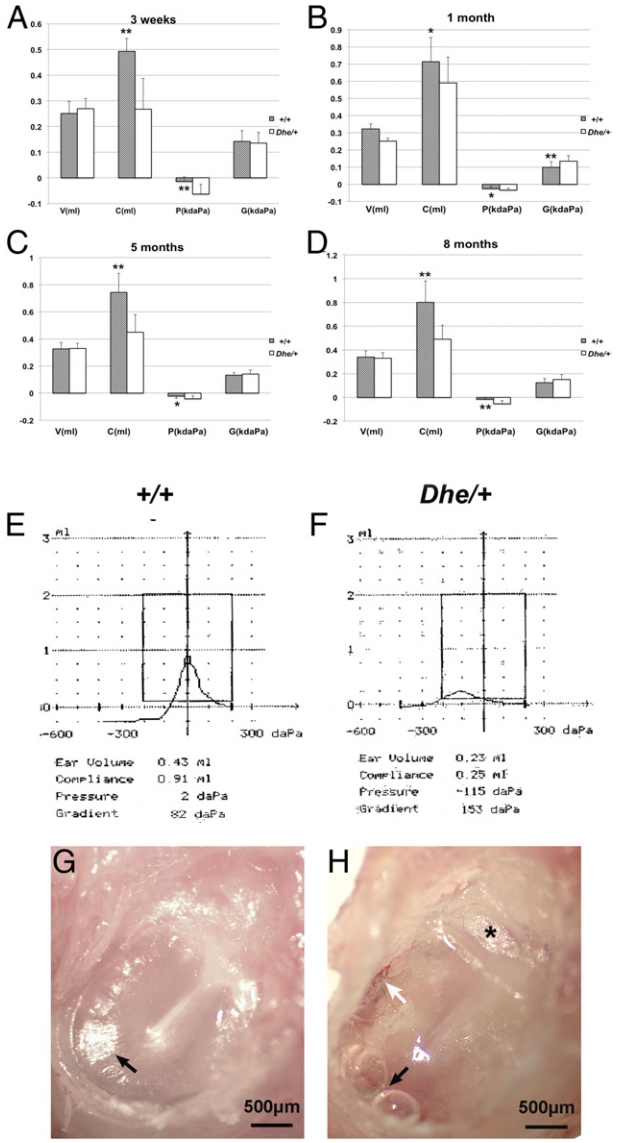


**Figure 2. A–D:** Comparison of mean values for each tympanometry parameter over a time course. At least 6 wild-type (+/+) and 6 *Lmna*$^{Dhe/+}$ mutant (*Dhe/+*) mice were assessed at each time point. **E** and **F:** Scanning tympanograms from wild-type and mutant mice at 5 months of age present, respectively, the normal A type curve (**E**, tall narrow curve with the peak near 0 daPa pressure) and the abnormal C type curve (**F**, low wide curve with the peak residing at negative pressure). **G** and **H:** Anatomical images under otoscopy of the same ears assessed in **E** and **F**, respectively. In the mutant mouse ear (**H**), tympanic membrane adherence (**asterisk**) was visible, and hyperemia (**white arrow**), hydrotympanum, and a shortened light cone (**black arrow**) were detected. A representative wild-type mouse ear (**G**) displays a normal tympanic membrane with a subuliform light cone on its anteroinferior quadrant (**black arrow**). Data are expressed as means ± SD. $*P < 0.05$; $**P < 0.01$. Scale bar = 500 $\mu$m.

(Figure 4, P–R). Littermate control mice exhibited no OM pathology and the eustachian tube grew with normal morphology (Figure 4, M–O). At 8 weeks in mutant mice, cells of the chronic inflammatory response pervaded the entire middle ear cavity (Figure 4V). The tympanic membrane thickened and retracted into the middle ear cavity (Figure 4W). The eustachian tube appeared distorted with dilation and exhibited poorly aligned and shortened or obsolescent cilia at this stage (Figure 4X). In contrast, wild-type control mice exhibited a clear middle ear cavity with a normally positioned tympanic membrane (Figure 4, S and T). Also in the wild type, the eustachian tube developed to a straight narrow shape and was covered with orderly, aligned, pseudostratified ciliated columnar epithelium (Figure 4U).

Diverse inflammatory manifestations were detected at different ages in *Lmna*$^{Dhe/+}$ mutant mice (Figure 5). Acute inflammatory cells and plasma fluids had infiltrated the middle ear cavity extensively at P30 (Figure 5, A and B). At older ages in *Lmna*$^{Dhe/+}$ mutant mice, from 2 months to 8 months, various manifestations of chronic suppurative middle ear inflammation occurred, with or without cholesteatoma. Cell infiltration and mucosal epithelium proliferation gradually appeared at 2 months (Figure 4V) and could progress to a much greater severity or develop encapsulated inflammation at older ages (Figure 5, C–H). Middle ear cholesteatoma was detected in some ears. Typical cholesterol crystals were revealed to be encysted by the hyperproliferative mucous epithelium and necrotic keratinizing squamous epithelium debris (Figure 5E). Local suppurative abscess formed in some of the middle ear cavities and collection of pus was enclosed by the surrounding hyperproliferative mucosal epithelium (Figure 5F). Proliferative goblet cells as detected by Mayer's mucicarmine staining revealed enhancement of the mucus-secreting ability in mutant mice (Figure 5H).

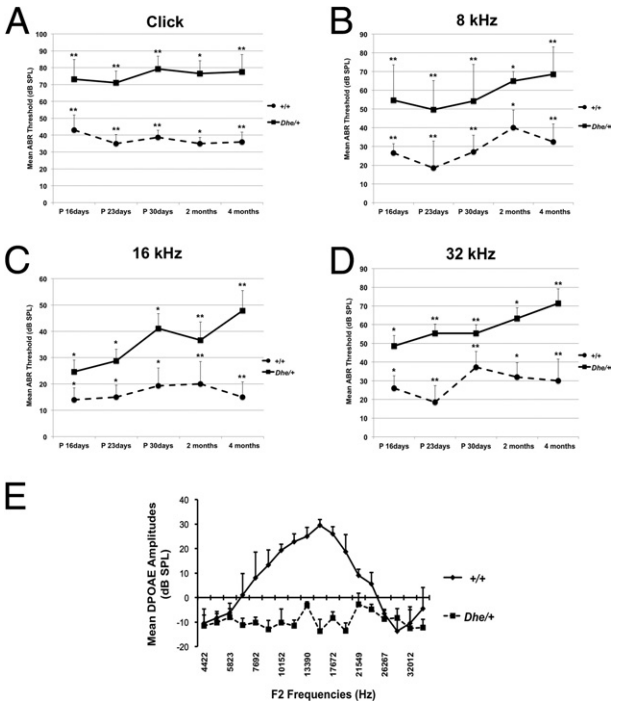


**Figure 3.** Time-course observation of ABR thresholds and DPOAE. **A–D:** ABR thresholds from the left ears of *Lmna*$^{Dhe/+}$ mutant (*Dhe/+*; $n = 34$) and wild-type mice (+/+; $n = 35$), tested at the ages of P16, P23, P30, 2 months, and 4 months. Compared with the wild-type control mice, the mutant mice exhibited significantly higher mean ABR threshold values at every stimulus frequency and at every time point. **E:** DPOAE measurement reveals lower amplitudes in mutant mice ($n = 4$), compared with wild-type mice ($n = 4$) at 3 months of age. Data are expressed as means ± SEM. $*P < 0.05$; $**P < 0.01$ Student's *t*-test.

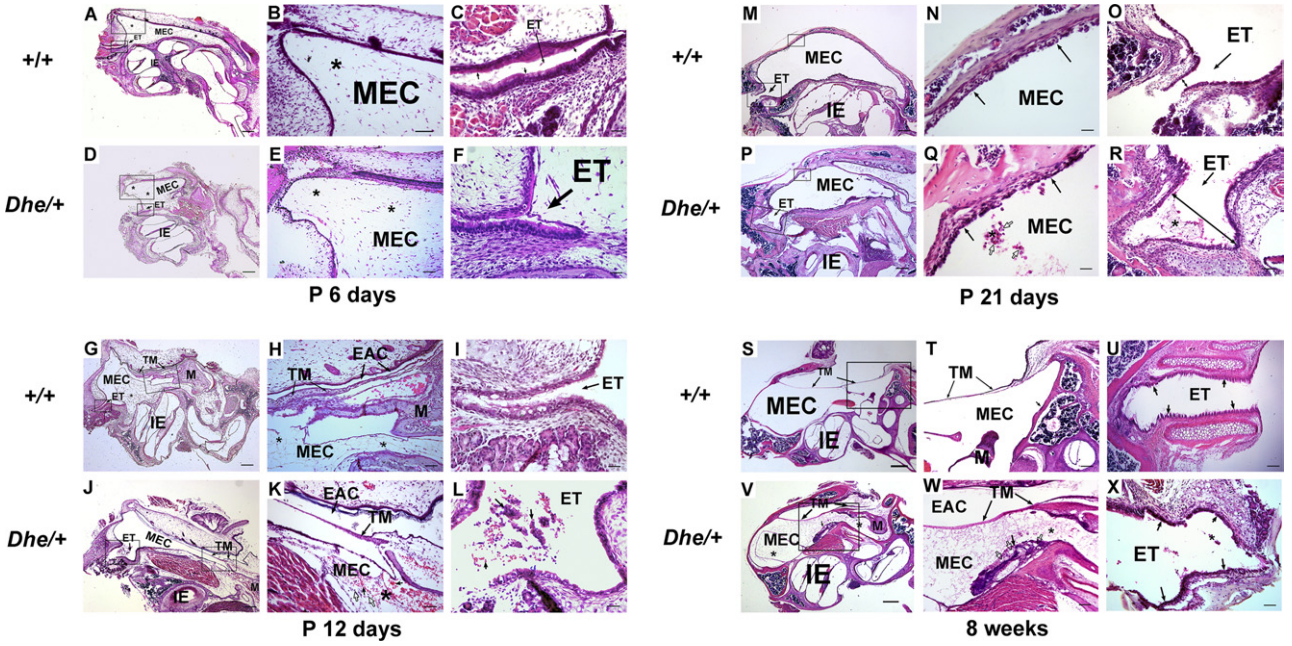


**Figure 4.** Time-course of OM onset and ET malformation. H&E histology over a time course revealed occurrence of OM inflammation and ET developmental malformation in *Lmna*$^{Dhe/+}$ mutant mice (*Dhe*/+), compared with the littermate control wild-type mice (+/+). $n = 4$ for each genotype at each time point. In each row, the **center** and **right** panels show magnified images corresponding to the two **boxed** regions in the **left** panel (excluding only **U** and **X**). **A–F:** Representative images of mice at P6. Sections exhibited no middle ear inflammation and no significant developmental disparity between the wild-type controls (**A**) and the mutant mice (**D**). Mesenchymal cells (**asterisks** in **A**, **B**, **D**, and **E**) were spread throughout the MEC. **C** and **F:** The ET was opened slightly and covered with pseudostratified ciliated columnar epithelium in both wild-type mice and mutants. **G–L:** Representative images of mice at P12. Onset of OM and dysplasia of ET occurred in the mutant mice. Mesenchymal cells still remain around the malleus in both groups (**asterisks** in **G**, **H**, **J**, and **K**). However, acute inflammatory response cells began to perfuse in the MEC of the mutant mice. Red blood cells (**black arrows** in MEC in **K**) and monocytes (**open arrows** in **K**) infiltrated in the mesenchymal cells. **H** and **K:** EACs were not fully open in mutants or controls. The TM of wild-type mice had developed to the normal three layers by this time, but was not fully developed in the mutant mice. The ET was enlarged in mutant mice (**L**), and debris of acute inflammatory response cells emerged (**asterisks**), compared with the narrow tubular ET shape and clear cavity in the wild-type mice (**I**). Red blood cells (**shortest arrow** in **L**) and monocyte masses (**longer arrows** in **L**) blocked the inner opening of the ET. **M–R:** Representative images of mice at P21. Ears of mutant mice continued to display OM and ET malformation. **M** and **P:** Mesenchymal cells disappeared, and middle ear cavitation was almost complete in both mutant and control mice. **M** and **N:** Wild-type mice (**N**) exhibited a clear MEC and healthy MEC mucosa (**arrows**), but mutant mice (**P**) exhibited inflammatory cell infiltration in MEC. **Q:** Detail of the MEC with thickened mucosa (**black arrows**) and inflammation (**asterisk**) in mutant mice; neutrophils infiltrated the MEC with exudates (**open arrows**). **O** and **R:** ET distortion was even more pronounced at P21. Dilation of ET interior diameter (**double-ended arrows**) was evident in mutant mice (**R**), compared with wild-type mice (**O**), and in the mutant mice (**R**) inflammatory exudate partially blocked the ET (**asterisk**). **S–X:** Representative images of mice at 8 weeks. **S** and **V:** Panoramic view of the bullae. In wild-type mice, neither middle ear inflammation nor TM retraction was detected (**S**), and the middle ear mucosa remained a thin layer and the TM retained normal position without retracting to the MEC (**T**). **V:** In mutant mice (**V**), inflammatory infiltration (**asterisks**) and debris (**short arrow**) pervaded the MEC, and TM retraction and thickness were accompanied by fibroblastic exudate (**asterisk**) and chronic inflammatory debris accumulation (**short black solid arrow** in MEC) with capillary hyperplasia (**open arrows**) in MEC (**W**). **U** and **X:** In ET at 8 weeks, wild-type mice (**U**) exhibited orderly, aligned, pseudostratified ciliated columnar epithelium (**arrows**). In mutant mice (**X**), the ET exhibited inflammatory cells (**asterisk**), epithelium with poor alignment, and shortened or obsolescent cilia (black **arrows**). Scale bars: 200 $\mu$m (**A**, **D**, **G**, **J**, **M**, **P**, **S**, and **V**); 100 $\mu$m (**T**, **U**, and **W**); 50 $\mu$m (**B**, **E**, **H**, **K**, **L**, **O**, **R**, and **X**); and 25 $\mu$m (**C**, **F**, **I**, **N**, and **Q**). EAC, external auditory canal; ET, Eustachian tube; IE, inner ear; M, malleus; MEC, middle ear cavity; TM, tympanic membrane.

We further measured the degree of pathology in OM by using five indices for semiquantitative evaluation as shown in Table 2. These data demonstrated that all of the *Lmna*$^{Dhe/+}$ mutant mice we tested exhibited OM and considerable inflammation, in contrast to wild-type control mice.

## *Scanning SEM Reveals Impaired Epithelial Cilia*

Using electron microscopy, we assessed the condition of middle ear pseudostratified ciliated columnar epithelium around the tympanic opening of the eustachian tube. At P21, pathological morphology was already apparent in the *Lmna*$^{Dhe/+}$ mutant mice, and by 10 weeks the cilia exhibited severe pathology indicative of OM progression (Figure 6). The epithelia from middle ears of control mice exhibited a thick lawn of orderly, evenly distributed cilia at both time points.

## *Immunofluorescent and RT-PCR Detection of Inflammatory Cytokines in the Middle Ear*

We stained middle ear paraffin sections from 8-week-old mice to determine whether protein levels of NF-$\kappa$B, TNF-$\alpha$, and TGF-$\beta$ were up-regulated as indicators of inflammation (Figure 7). The expression of NF-$\kappa$B, TGF-$\beta$, and TNF-$\alpha$ were all up-regulated in *Lmna*$^{Dhe/+}$ mutant mice which also exhibited thickened epithelial walls and inflammatory cell infiltration, compared with controls (Figure 7, E, K, and Q). The staining intensities for all three antibodies were stronger in the *Lmna*$^{Dhe/+}$ mutant tissues than in wild-type controls. Under higher magnification, the staining intensity of all three antibodies appeared stronger in the middle ear mucosa (Figure 7, E, K, and Q) and was localized to the cytoplasm of middle ear epithelial cells (Figure 7, F, L, and R) of the mutant mice, compared with weaker staining in wild-type mice. The inflammatory cells in the middle ear

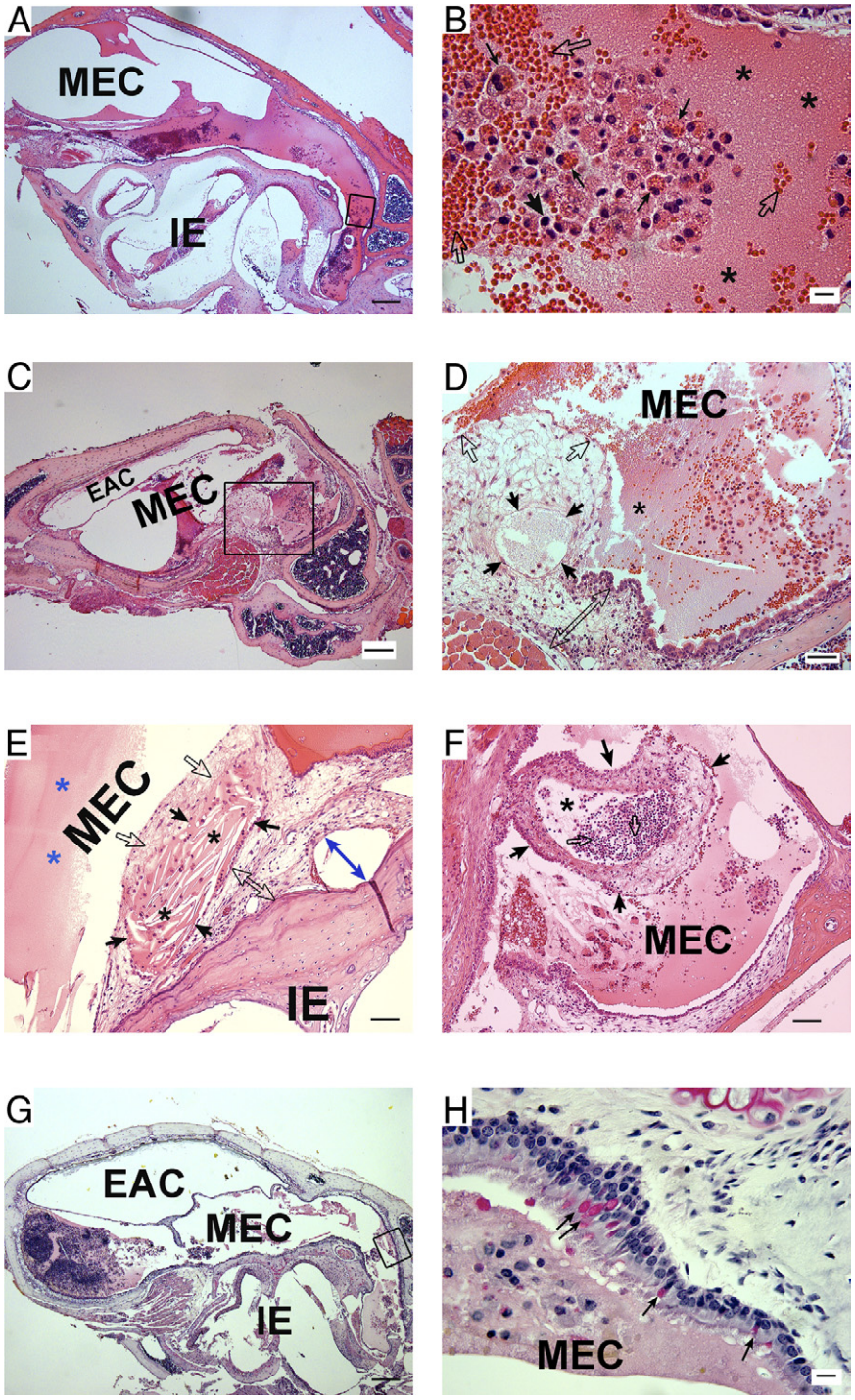


**Figure 5.** Diverse manifestation of middle ear inflammation in *Lmna*$^{Dhe/+}$ mutant mice at different ages. **A–F:** Representative H&E histology shows the diversity of middle ear inflammation at 30 days (**A** and **B**), 3 months (**C** and **D**), and 8 months (**E** and **F**) of age in mutant mice. **G** and **H:** Mayer's mucicarmine staining of the middle ear mucosa revealed goblet cells. **A:** Acute inflammation was observed in a section from a P30 mutant mouse. **B:** At higher magnification, the **boxed** region in **A** revealed acute inflammatory exudate. Masses of erythrocytes (**open arrows**) extravasated to the middle ear cavity and were partially engulfed by macrophages (**thin black arrows**). Blood plasma together with fibrin (**asterisks**) comprised a large portion of the effusion. A few basophils were also detected (**thick black arrow**). **C:** Representative images demonstrate chronic inflammation in mice at the age of 3 months. **D:** At higher magnification, the **boxed** region in **C** displays a detailed view of the cell proliferation and infiltration. Exudates of blood plasma and fibrin (**asterisks**) were still evident at this time point. Middle ear mucosal epithelium was hyperproliferative (**open arrows** and **open double-ended arrow**) and even included locally enclosed exudates (**black arrows**). **E** and **F:** Two typical examples of chronic inflammation from mice at the age of 8 months. **E:** Middle ear cholesteatoma formation. Cholesterol crystals (**black asterisks**) were encysted by the hyperproliferative mucous epithelium of the MEC (**black arrows**) and necrotic keratinizing squamous epithelium debris (**open arrows**). Mucosal epithelium had hyperproliferated (**open double-ended arrow**) or desquamated from the bone (**blue double-ended arrow**). Amorphous eosinophilic substance exhibited plasma fluid exudate (**blue asterisks**). **F:** Local suppurative abscess formation in the middle ear cavity (**asterisk**). Collection of pus consisted mainly of neutrophils (**open arrows**); dead cells and fluid were enclosed by surrounding hyperproliferative tissues of the mucosal epithelium (**black arrows**). **G:** Mayer's mucicarmine staining of the middle ear. **H:** At higher magnification, the **boxed** region in **G** reveals the typical proliferation of goblet cells, stained red (**arrows**). Scale bars: 200 $\mu$m (**A**, **C**, and **G**); 50 $\mu$m (**D–F**); and 10 $\mu$m (**B** and **H**). EAC, external auditory canal; IE, inner ear; MEC, middle ear cavity.

cavities of mutant mice also exhibited strong cytoplasmic staining intensity of all three antibodies (Figure 7, E, K, and Q).

Detection of protein expression was also confirmed by RT-PCR for up-regulation of TGF-$\beta$ (Figure 8). *Gapdh*-correlated, semiquantitative RT-PCR analysis revealed that the TGF-$\beta$ mRNA expression levels in the middle ear in three 21-day-old *Lmna*$^{Dhe/+}$ mutant mice were increased, compared with three wild-type littermate control mice ($P < 0.05$). These data confirm the protein expression data indicating active inflammation in the ears of *Lmna*$^{Dhe/+}$ mutant mice.

## *Blood Levels of Calcium and Phosphorus Indicate Abnormal Levels of Serum Ions in* Lmna$^{Dhe/+}$ *Mutant Mice*

Because hyperphosphatemia has been associated with laminopathy in humans,[14] we investigated the se-

**Table 2.** Pathology in Middle Ears of Wild-Type and *Lmna*$^{Dhe/+}$ Mutant Mice

| Mouse genotype and ID | Age | Middle ear effusion | Inflammatory cell infiltration | Tissue debris | Tissue proliferation | Goblet cells | Inner ear effusion | Score*†‡ |
|---|---|---|---|---|---|---|---|---|
| Wild type (+/+) littermate control mice | | | | | | | | |
| 1 | P12 | − | − | + | − | − | − | 1 |
| 2 | P12 | − | − | − | − | − | − | 0 |
| 3 | P12 | − | − | − | − | − | − | 0 |
| 4 | P12 | − | − | − | − | − | − | 0 |
| 5 | P21 | − | − | − | − | − | − | 0 |
| 6 | P21 | − | − | − | − | − | − | 0 |
| 7 | P21 | − | − | − | − | − | − | 0 |
| 8 | P21 | ++ | ++ | + | ++ | + | − | 8 |
| 9 | 8 wk | − | − | − | − | − | − | 0 |
| 10 | 8 wk | − | − | − | − | − | + | 1 |
| 11 | 8 wk | − | − | − | − | − | − | 0 |
| 12 | 8 wk | − | − | − | − | − | − | 0 |
| Mutant *Lmna*$^{Dhe/+}$ mice | | | | | | | | |
| 13 | P12 | ++ | ++ | ++ | ++ | + | − | 9 |
| 14 | P12 | + | + | ++ | + | − | − | 5 |
| 15 | P12 | ++ | ++ | + | + | − | − | 6 |
| 16 | P12 | + | ++ | ++ | + | − | − | 6 |
| 17 | P21 | +++ | ++ | + | ++ | + | − | 9 |
| 18 | P21 | +++ | ++ | ++ | ++ | + | − | 10 |
| 19 | P21 | +++ | ++ | ++ | ++ | + | − | 10 |
| 20 | P21 | ++ | +++ | + | + | + | − | 8 |
| 21 | 8 wk | ++ | +++ | ++ | +++ | ++ | − | 12 |
| 22 | 8 wk | +++ | +++ | +++ | +++ | ++ | + | 15 |
| 23 | 8 wk | +++ | +++ | ++ | +++ | ++ | − | 13 |
| 24 | 8 wk | +++ | +++ | ++ | ++ | ++ | − | 12 |
| 25 | 4 mo§ | +++ | +++ | ++ | +++ | +++ | − | 14 |
| 26 | 4 mo§ | ++ | ++ | ++ | +++ | +++ | − | 12 |
| 27 | 4 mo§ | +++ | +++ | +++ | +++ | +++ | − | 15 |
| 28 | 8 mo§ | +++ | +++ | +++ | +++ | +++ | − | 15 |
| 29 | 8 mo§ | +++ | +++ | +++ | +++ | +++ | − | 15 |
| 30 | 8 mo§ | + | +++ | +++ | +++ | +++ | − | 13 |

The degree of pathological severity was evaluated in the middle ears of wild-type (+/+) and mutant (*Lmna*$^{Dhe/+}$) mice on the basis of middle ear effusion, inflammatory cell infiltration, tissue debris, tissue proliferation, goblet cells, and inner ear effusion. Severity of pathology was scored as follows: −, absence of pathology in the middle or inner ear; +, very scarce pathology; ++, prevalent pathology, but not spread throughout the entire middle or inner ear; +++, pathology infiltrating the entire middle or inner ear.

*The maximum possible score per mouse was 18 points (1 point for each +).

†The total scored rate (199/324) of the 18 *Lmna*$^{Dhe/+}$ mutant mice was significantly higher than that (10/216) of the 12 wild-type mice ($P < 0.01$, $\chi^2$ test).

‡In the *Lmna*$^{Dhe/+}$ mutant mice, score rates progressively rose with age. There was no statistically significant difference between P12 (26/72) and P21(37/72) scores, but 8-week scores (52/72) were significantly higher than those at P21, and the combined 4- and 8-month scores (84/108) were significantly higher than the 8-week scores ($P < 0.01$, $\chi^2$ test).

§Six older *Lmna*$^{Dhe/+}$ mutant mice were scored at 4 and 8 months, to evaluate the inflammatory tendency.

rum levels of phosphorus and calcium in adult *Lmna*$^{Dhe/+}$ mice to determine whether these mice display features of laminopathy. Furthermore, some laminopathies in humans exhibit a phenotype in females, but not necessarily in males.[15] The mean serum calcium in female wild-type mice was significantly lower than in male wild-type mice (Table 3). However, the mutant mice (*Lmna*$^{Dhe/+}$) of either sex exhibited calcium serum levels intermediate between the male and female wild-type levels. Serum phosphorus in mutant female mice (*Lmna*$^{Dhe/+}$) was detected at significantly higher levels (7.5 ± 0.76) than that of the wild-type mice (5.2 ± 0.35). Also, within the female population, the mutant mice exhibited a lower calcium/phosphorus ratio (1.16 ± 0.12) than the wild-type mice (1.61 ± 0.17). Mutant female mice had a higher value for the Ca × P product (65.25 ± 6.05 mg$^2$/dL$^2$), compared with wild-type female or mutant male mice. Taken together, these data indicate that a reduced calcium/phosphorus ratio in mutant female mice is the result of phosphorus increase, rather than a calcium decrease.

### *Cell Counting Revealed No Anomaly of Macrophage Migration* in Vivo *in* Lmna$^{Dhe/+}$ *Mice*

To evaluate the effect of *LMNA* mutation on macrophage migration *in vivo*, we measured macrophages from the peritoneal cavity 3 days after thioglycollate broth injection from 4-month-old wild-type control mice and *Lmna*$^{Dhe/+}$ mutant mice (3 female and 3 male in each group). In this assay, the numbers of macrophages were $4.58 \times 10^6$/mL (SE = $1.3 \times 10^5$) in wild-type mice and $5.01 \times 10^6$/mL (SE = $2.6 \times 10^5$) ($P = 0.787$) in mutant mice. The result revealed no statistically significant difference in the number of peritoneal macrophages elicited by thioglycollate, neither between the sexes nor between the two groups of mice.

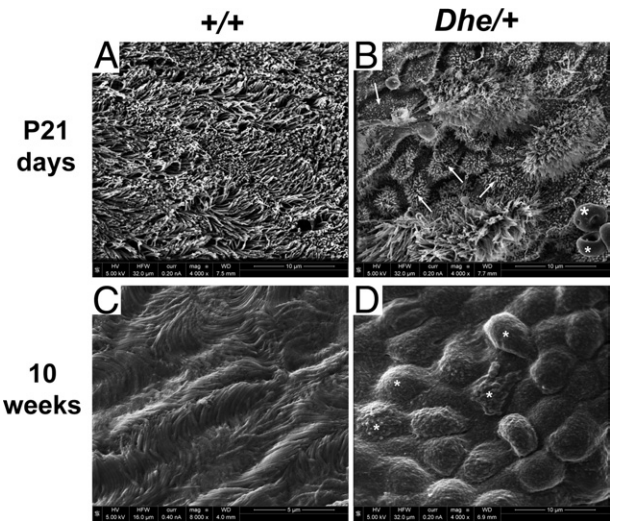


**Figure 6.** Scanning electron micrographs of middle ear epithelium near the ET. Shown are representative images from wild-type (+/+) and *Lmna*$^{Dbe/+}$ mutant (*Dbe/+*) mice at P21 and 10 weeks, displaying middle ear pseudostratified ciliated columnar epithelium around the tympanic opening of the eustachian tube. **A** and **C:** Normal morphology of the cilia in the mucociliary epithelium of a control mouse. **B:** Impaired and disrupted epithelium with atrophic shortened cilia (**arrows**) in a mutant mouse, with red blood cells on the epithelial surface (**asterisks**). **D:** Epithelium with impaired, deformed cilia (**asterisks**). Scale bars: 10 $\mu$m (**A**); 5 $\mu$m (**B–D**).

The present study suggests that macrophage migration is not dependent on *LMNA* mutation.

### *Immunodetection of Nuclear Lamina Morphology and TGF-β and TNF-α Expression in Peritoneal Macrophages*

Peritoneal macrophages reflect some aspects of the host immune status. To determine whether the nuclear lamina morphology or meshwork of the nuclear envelope appeared consistent with laminopathy, and whether macrophages appeared activated, consistent with infection in *Lmna*$^{Dhe/+}$ mice, we stained peritoneal macrophages from 4-month-old mice with anti-LMNA, anti-TGF-$\beta$, and anti-TNF-$\alpha$ (Figure 9). Immunofluorescence revealed a compact, plump, and even nuclear lamina meshwork in wild-type mice (Figure 9A), but in mutants the nuclear meshwork appeared rugous, disintegrative, or even collapsed (Figure 9C). Nuclear volumes were notably larger in mutant than in wild-type macrophages. TGF-$\beta$ and TNF-$\alpha$ were both expressed in the macrophages from *Lmna*$^{Dhe/+}$ mice and expression was localized to both the nucleus and the cytoplasm and, together with the cell enlargement, indicated macrophage activation consistent with infection in these mice.

## *Discussion*

Recent study on mouse models for OM reveals that genetic predisposition is becoming recognized as an important pathogenesis factor of the disease.[16] Multiple factors leading to OM include infection, anatomical factors, immunological status, environmental factors, and genetic predisposition, which refer to the genetic pathogenesis underlying OM. A previous study confirmed that the *Lmna*$^{Dhe}$ mutation in mice leads to craniofacial dysmorphology resembling that in humans with mandibuloacral dysplasia, and defects of the skin and hair found in Hutchinson-Gilford progeria syndrome.[7] A recent investigation also revealed that patients with Hutchinson-Gil-

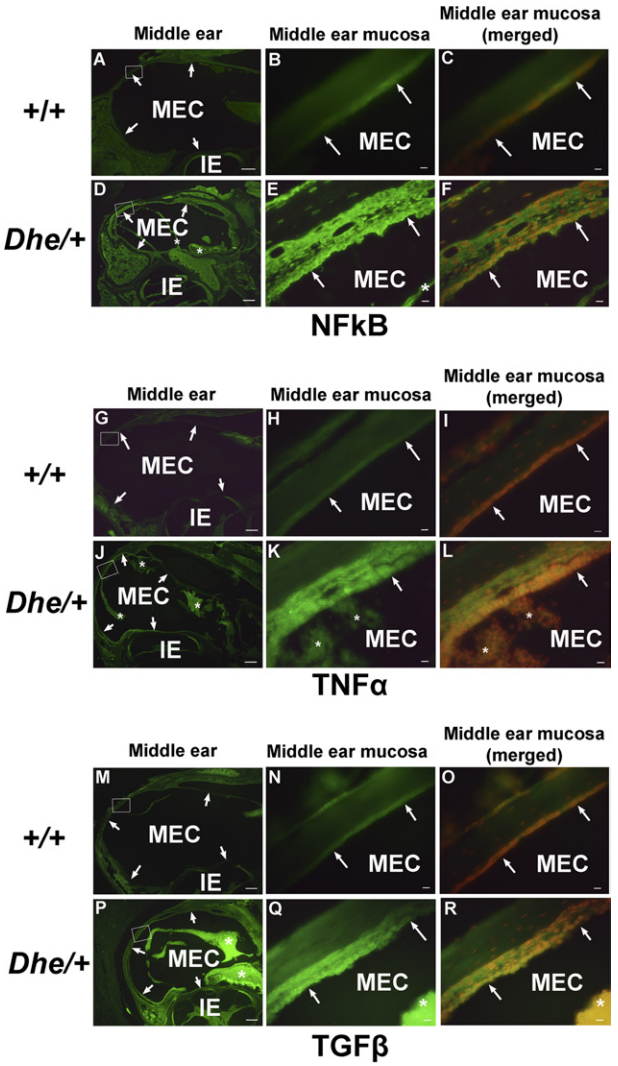


**Figure 7.** Immunofluorescent detection of proinflammatory proteins NF-κB, TNF-α, and TNF-β in middle ear tissue. Representative middle ear sections from 8-week-old wild-type (+/+) and *Lmna*$^{Dbe/+}$ mutant (*Dbe/+*) mice, stained with anti-NF-κB (**A–F**), anti-TNF-α (**G–L**), and anti-TGF-β (**M–R**) antibodies and revealed with Alexa Fluor 488 (green). $n$ = 6/group. Images at the **left** (**A**, **D**, **G**, **J**, **M**, and **P**) reveal gross morphology of the middle and inner ears; **arrows** indicate borders of the middle ear cavity and **asterisks** indicate inflammatory tissues. Images in the **middle** (**B**, **E**, **H**, **K**, **N**, and **Q**) show the regions of interest (**boxed** in the corresponding panels at **left**) at higher magnification. In the wild-type mice (**B**, **H**, and **N**), the middle ear mucosa remains a normal thin layer (**arrows** indicate position and morphology of the middle ear mucosa), with faint staining in the cytoplasm of the epithelium. The mutant mice (**E**, **K**, and **Q**) exhibit thickened epithelia (**arrows**) and inflammatory tissues (**asterisks**) in the middle ear. Merged images at the **right** (**C**, **F**, **I**, **L**, **O**, and **R**) correspond to the panels in the middle; propidium iodide counterstain (red; counterstain images not shown separately) was used to reveal nuclei. **E**, **K**, and **Q**: In mutant mice, inflammatory cells (**asterisks**) in the middle ear cavities also exhibited strong cytoplasmic staining. Scale bars: 200 $\mu$m (left: **A**, **D**, **G**, **J**, **M**, and **P**); 10 $\mu$m (middle and right: **B**, **C**, **E**, **F**, **H**, **I**, **K**, **L**, **N**, **O**, **Q**, and **R**). IE, inner ear; MEC, middle ear cavity.

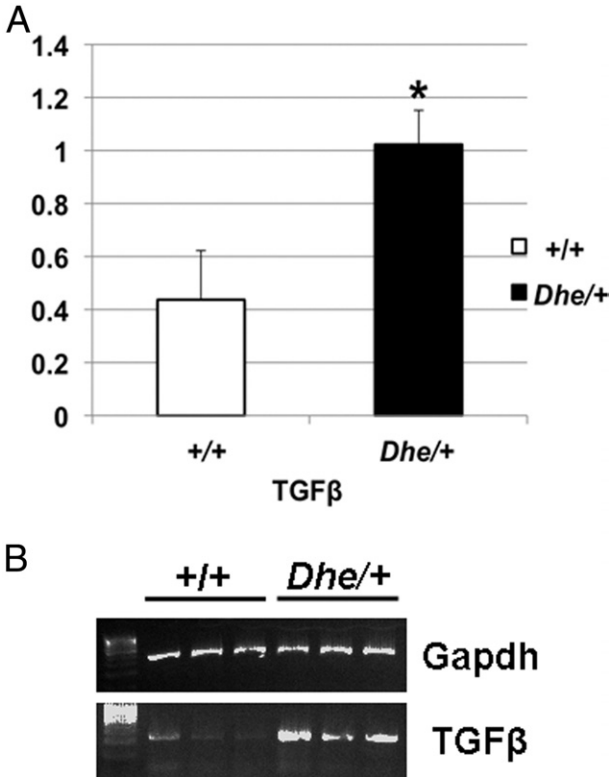


**Figure 8.** RT-PCR detection of TGF-$\beta$ in middle ear tissue of *Lmna*$^{Dhe/+}$ mutant (*Dhe/+*) and wild-type (+/+) mice. **A:** Results of semiquantitative PCR for TGF-$\beta$ were normalized to *Gapdh* expression levels, digitized, and plotted as mean expression levels for comparison. Mutant mice expressed approximately twice the mean level of TGF-$\beta$ transcript in middle ear tissue, compared with wild-type mice. **B:** Agarose gel of RT-PCR products from the samples from which the means in **A** were derived. $^*P < 0.05$. $n = 3$ mice per genotype.

ford progeria syndrome often exhibited low-frequency conductive hearing loss and deformity of auriculae and external ear canals.[6,14] The present study examined the functional and morphological auditory consequences of *Lmna*$^{Dhe}$ mutation in mice and revealed malformation and altered positioning of the eustachian tube, accompanied by OM. Together with measurement of serum calcium and phosphorus abnormality, and nuclear defects of peritoneal macrophages, we further associated the *Lmna*$^{Dhe}$ mutation with pathology of OM and other pathological features of laminopathies.

The eustachian tube is composed of a bony portion, cartilaginous portion, and adjunctional portion. The bony portion of the eustachian tube functions in ventilation and clearance of secretions and is lined by pseudostratified ciliated columnar epithelium, with an antigravitational direction of drainage.[17] Bacteria that commonly infect the middle ear are normally resident in the nasopharynx. These bacteria proliferate and invade the middle ear via the eustachian tube under circumstances of eustachian tube dysfunction when ventilation and clearance are poor. Proper morphology and position enables the eustachian tube to function properly and protect the middle ear.[13] In *Lmna*$^{Dhe/+}$ mice, the eustachian tube grows to a shortened, broad shape along with a positional change. The intersection angle between the bilateral eustachian tube increases, positioning the bony part of the eustachian tube in a more horizontal orientation. A recent prospective study in human OM revealed that, from the age of 2 years, eustachian tubes with a horizontal orientation impaired the clearance, ventilation, and protection of the middle ear.[18] Furthermore, obstruction of the eustachian tube orifice by adjacent nasopharynx tissue can also contribute to onset of OM.[19,20] Close proximity or a fused gap between the nasopharynx roof and the palate bone may obstruct the orifice of the eustachian tube in *Lmna*$^{Dhe/+}$ mutant mice. Both structural malformation and dysfunction of eustachian tube may impede clearance of secretions in the middle ear with a risk of ciliary damage.[4] The present study is the first to demonstrate a critical role for *LMNA* mutation in the onset of OM related to malformation of the eustachian tube.

Pathological investigation revealed dilation and distortion of the bony part of the eustachian tube and, in all *Lmna*$^{Dhe/+}$ mice, evidence of OM beginning at P12 with associated pathologies progressively worsening. Inflammation evolved from acute OM, to OM with effusion, to chronic suppurative OM, with or without cholesteatoma. The phenotypic process of OM is consistent with human OM.[21,22] Hearing assessment in mutant mice revealed lower compliance of more negative value in tympanograms, compared with normal controls. ABR thresholds revealed that hearing loss was significantly more pronounced at lower frequencies. In human patients, lower peak of compliance in the negative pressure zone supports the diagnosis of OM.[23] Also, lower frequencies of ABR threshold are more compromised than higher ones in human OM.[18] DPOAE confirmed lower amplitudes in *Lmna*$^{Dhe/+}$ mice. Middle ear pathology such as OM can alter sound transfer to the inner ear and result in parallel shifts in DPOAE.[24]

The mutant mice exhibited evidence of inflammation as increased protein levels of TNF-$\alpha$, NF-$\kappa$B, and TGF-$\alpha$ in the middle ear, consistent with the inflammation observed in mouse and human OM.[25–27] We further investigated the TGF-$\beta$ mRNA level in the middle ear because this

**Table 3.** Serum Levels of Phosphorus and Calcium in Adult *Lmna*$^{Dhe/+}$ Mice

| Measure | +/+ Female | *Dhe*/+ Female | +/+ Male | *Dhe*/+ Male |
|---|---|---|---|---|
| Calcium (mg/dL) | 8.33 ± 0.31$^\dagger$ | 8.7 ± 0.12 | 9.3 ± 0.12$^\dagger$ | 8.9 ± 0.30 |
| Phosphorus (mg/dL) | 5.2 ± 0.35* | 7.5 ± 0.76* | 6.3 ± 0.99* | 5.9 ± 0.23* |
| Ca/P ratio | 1.61 ± 0.17* | 1.16 ± 0.12* | 1.50 ± 0.20 | 1.50 ± 0.11 |
| Ca × P product (mg$^2$/dL$^2$) | 45.36 ± 2.04* | 65.25 ± 6.05*$^\dagger$ | 58.15 ± 9.92 | 52.57 ± 0.65$^\dagger$ |

Data are presented as means ± SD.
$^*P < 0.05$, wild type (+/+) versus mutant (*Dhe/+*). $^\dagger P < 0.05$, male versus female within genotype.

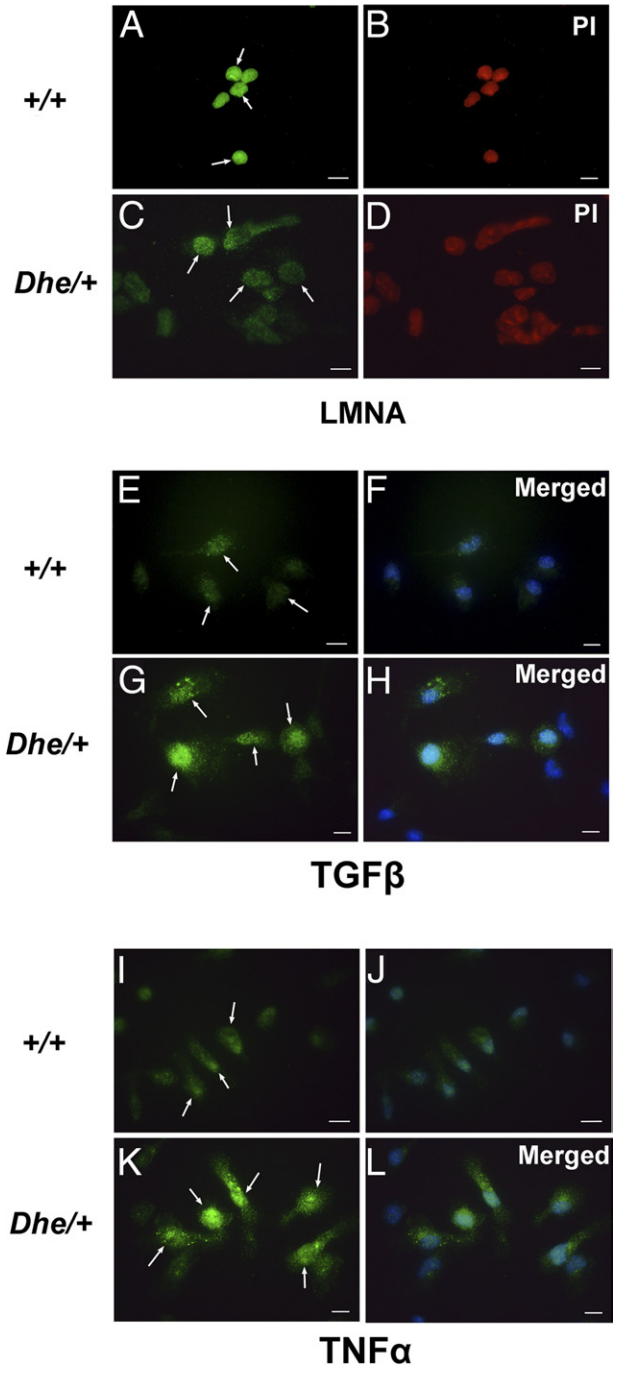


**Figure 9.** Detection of nuclear lamina morphology and expression disparity of TGF-$\beta$ and TNF-$\alpha$ in peritoneal macrophages of wild-type (+/+) and *Lmna*$^{Dhe/+}$ mutant (*Dhe*/+) mice. Shown are representative images of immunofluorescent staining of peritoneal macrophages of wild-type and mutant mice. **A–D:** Staining with anti-LMNA antibody reveals nuclear lamina morphology in peritoneal macrophages. Note the compact, plump, and even meshwork of the nuclear envelope, apparent as green fluorescence (**arrows**) in wild-type cells (**A**), compared with the rugous, disintegrative or even collapsed envelope (**arrows**) in *Dhe*/+ cells (**C**). Nuclei were larger in mutant than in wild-type cells. **B** and **D:** Nuclear localization was confirmed by counterstaining with propidium iodide (red). **E–L:** Peritoneal macrophages were stained with anti-TGF-$\beta$ (**E–H**) or anti-TNF-$\alpha$ (**I–L**) antibody, revealing expression of these proteins in mutant macrophages, but with only faint staining (if any) in those from wild-type macrophages. Again, macrophages exhibited enlargement in the mutant mice, and expression of both TGF-$\beta$ and TNF-$\alpha$ was observed in both the cytoplasm and the nucleus (**arrows**). **F**, **H**, **J**, and **L:** Merged images corresponding to images **E**, **G**, **I**, and **K**, respectively. DAPI counterstain (blue; counterstain images not shown separately) was used to reveal nuclei. Scale bar = 10 $\mu$m.

protein not only plays a role in inflammation but also is an important modulator of bone formation, induction, and repair. TGF-$\beta$ controls proliferation, cellular differentiation, epithelial mesenchymal transformation,[28,29] and other functions in many cell types. The TGF-$\beta$ signaling pathway dictates craniofacial development and plays multiple and critical roles during all stages of tooth development.[30] The TGF-$\beta$-Smad signaling pathway is affected in the human laminopathies mandibuloacral dysplasia type A and osteopoikilosis, which are characterized by skeletal dysplasia.[31] TGF-$\beta$ can be overexpressed as a result of cellular responses that also recruit bone morphogenic proteins to the inner nuclear membrane.[32]

TGF-$\beta$ also plays a crucial role in regulation of cell cycle, another function that could be of consequence in the *Lmna*$^{Dhe/+}$ mouse. TGF-$\beta$ triggers p15 and p21 protein synthesis, which block the cyclin:CDK complex. Retinoblastoma protein phosphorylation (pRb) is then effected.[33] Many data indicate that expression of components of the pRb-MyoD signaling cascade is disrupted in both animal models of Emery-Dreifuss muscular dystrophy type 1 (EDMD1), and in EDMD2 and EDMD3 skeletal defects.[34] Moreover, laminopathies primarily affect tissues of mesenchymal origin and can modulate TGF-$\beta$–dependent signaling through interaction with protein phosphatase 2A (PP2A).[35] A previous study identified the craniofacial defects of *Lmna*$^{Dhe/+}$ mutant mice.[7] The present study supplies further evidence of the malformation and malposition of the eustachian tube and adjacent nasopharynx tissues. We suggest that the TGF-$\beta$ signaling pathway may play a role in development of craniofacial phenotype in *Lmna*$^{Dhe/+}$ mutant mice.

To investigate factors related to pathological features of laminopathies in *Lmna*$^{Dhe/+}$ mutant mice, we assessed serum calcium and phosphorus. Phosphate is widely distributed in the body and is involved in energy metabolism, cell signaling, nucleic acid synthesis, and maintenance of acid-base balance. Hyperphosphatemia is a critical factor in mammalian aging, by virtue of its role in skeletal deformity, cardiac and renal diseases, hypogonadism, and infertility. The phenotype of the mouse model of hyperphosphatemia, Klotho-knockout mice (*klotho*$^{-/-}$), is manifested as premature aging, the features of which can be ameliorated by hypophosphorus diet and genetic manipulation.[36] When hyperphosphatemia occurs in conjunction with increased calcium $\times$ phosphate product levels, an 18% to 39% higher risk of pathology has been demonstrated.[37] In Hutchinson–Gilford progeria syndrome, serum phosphorus levels in patients are elevated.[14] We found an increase of serum phosphorus in all *Lmna*$^{Dhe/+}$ mutant mice tested and of the calcium $\times$ phosphate product specifically in female mutant mice. Female mutants also have lower reproductive potential than male mutants,[7] but share other pathological features with males. The functional consequences of the increased calcium $\times$ phosphate product in female mutants need further investigation.

We also investigated the function of peritoneal macrophages *in vivo*, which may reflect some aspects of the host immune status, in *Lmna*$^{Dhe/+}$ mutant mice. Macro-

phages function in both innate and adaptive immunity of vertebrates.[38] Peritoneal macrophages are resident cells within the peritoneal cavity.[39] In previous studies of *Lmna*$^{Dhe/+}$ mice, abnormal morphology of the nuclear laminae in osteoblasts[7] and in fibroblasts[8] was reported. Although the assay of macrophage migration *in vivo* found no abnormity in *Lmna*$^{Dhe/+}$ mutant mice, the present study revealed structural lesions of the nuclear laminae in macrophages. Furthermore, protein levels of TGF-$\beta$ and TNF-$\alpha$ were increased in the peritoneal macrophages in *Lmna*$^{Dhe/+}$ mutant mice, both of which are chiefly produced by activated macrophages and play a primary role in regulating immune cells.[40–42]

The *Lmna*$^{Dhe/+}$ mutant mice provide a new dominant hereditary model of the genetic contribution to the onset of OM and laminopathies. We describe for the first time the malformation of the nasopharynx tissue in *Lmna*$^{Dhe/+}$ mutant mice, which has not been reported in other mouse models of OM. Including the early-onset malformation of the eustachian tube, the *Lmna*$^{Dhe/+}$ mutant mice morphologically mimic human OM. All of the *Lmna*$^{Dhe/+}$ mutant mice we studied revealed spontaneous development of OM after the age of P12 days, and all pathological manifestations of human OM have been detected in these mutants. OM became severe with age. Abnormalities of serum calcium and phosphorus and nuclear defects of peritoneal macrophages reflected to some extent similar pathological features of human laminopathies. Further studies are warranted to elucidate how the *Lmna*$^{Dhe/+}$ mutation is involved in the pathological features of laminopathies, including a possible linkage of these to OM. We provide an important step toward understanding the pathogenesis of OM related to *LMNA* mutation and to some pathological features of laminopathies. This knowledge will supply new perspective on treatment and prevention for both OM and laminopathies.

## Acknowledgments

We thank Bin Yang, Qiuhong Huang, Frank Zhang, and Linda Le for their technical assistance and Dr. Leah Rae Donahue (The Jackson Laboratory) for providing the initial breeding pairs of the *Dhe* mice.

## References

1. Vergison A, Dagan R, Arguedas A, Bonhoeffer J, Cohen R, Dhooge I, Hoberman A, Liese J, Marchisio P, Palmu AA, Ray GT, Sanders EA, Simões EA, Uhari M, van Eldere J, Pelton SI: Otitis media and its consequences: beyond the earache. Lancet Infect Dis 2010, 10:195–203
2. Park K, Ueno K, Lim DJ: Developmental anatomy of the eustachian tube and middle ear in mice. Am J Otolaryngol 1992, 13:93–100
3. Noben-Trauth K, Latoche JR: Ectopic mineralization in the middle ear and chronic otitis media with effusion caused by RPL38 deficiency in the Tail-short (Ts) mouse. J Biol Chem 2011, 286:3079–3093
4. Depreux FF, Darrow K, Conner DA, Eavey RD, Liberman MC, Seidman CE, Seidman JG: Eya4-deficient mice are a model for heritable otitis media. J Clin Invest 2008, 118:651–658
5. Brown CA, Lanning RW, McKinney KQ, Salvino AR, Cherniske E, Crowe CA, Darras BT, Gominak S, Greenberg CR, Grosmann C, Heydemann P, Mendell JR, Pober BR, Sasaki T, Shapiro F, Simpson DA, Suchowersky O, Spence JE: Novel and recurrent mutations in lamin A/C in patients with Emery-Dreifuss muscular dystrophy. Am J Med Genet 2001, 102:359–367
6. Guardiani E, Zalewski C, Brewer C, Merideth M, Introne W, Smith AC, Gordon L, Gahl W, Kim HJ: Otologic and audiologic manifestations of Hutchinson-Gilford progeria syndrome. Laryngoscope 2011, 121:2250–2255
7. Odgren PR, Pratt CH, Mackay CA, Mason-Savas A, Curtain M, Shopland L, Ichicki T, Sundberg JP, Donahue LR: Disheveled hair and ear (Dhe), a spontaneous mouse Lmna mutation modeling human laminopathies. PLoS One 2010, 5:e9959
8. Pratt CH, Curtain M, Donahue LR, Shopland LS: Mitotic defects lead to pervasive aneuploidy and accompany loss of RB1 activity in mouse LmnaDhe dermal fibroblasts. PLoS One 2011, 6:e18065
9. Zheng QY, Johnson KR, Erway LC: Assessment of hearing in 80 inbred strains of mice by ABR threshold analyses. Hear Res 1999, 130:94–107
10. Yang B, Tian C, Zhang ZG, Han FC, Azem R, Yu H, Zheng Y, Jin G, Arnold JE, Zheng QY: Sh3pxd2b mice are a model for craniofacial dysmorphology and otitis media. PLoS One 2011, 6:e22622
11. Han F, Yu H, Tian C, Li S, Jacobs MR, Benedict-Alderfer C, Zheng QY: Role for Toll-like receptor 2 in the immune response to Streptococcus pneumoniae infection in mouse otitis media. Infect Immun 2009, 77:3100–3108
12. Chen M, Ona VO, Li M, Ferrante RJ, Fink KB, Zhu S, Bian J, Guo L, Farrell LA, Hersch SM, Hobbs W, Vonsattel JP, Cha JH, Friedlander RM: Minocycline inhibits caspase-1 and caspase-3 expression and delays mortality in a transgenic mouse model of Huntington disease. Nat Med 2000, 6:797–801
13. Trune DR, Zheng QY: Mouse models for human otitis media. Brain Res 2009, 1277:90–103
14. Merideth MA, Gordon LB, Clauss S, Sachdev V, Smith AC, Perry MB, Brewer CC, Zalewski C, Kim HJ, Solomon B, Brooks BP, Gerber LH, Turner ML, Domingo DL, Hart TC, Graf J, Reynolds JC, Gropman A, Yanovski JA, Gerhard-Herman M, Collins FS, Nabel EG, Cannon RO 3rd, Gahl WA, Introne WJ: Phenotype and course of Hutchinson-Gilford progeria syndrome. N Engl J Med 2008, 358:592–604
15. Broers JL, Ramaekers FC, Bonne G, Yaou RB, Hutchison CJ: Nuclear lamins: laminopathies and their role in premature ageing. Physiol Rev 2006, 86:967–1008
16. Zheng QY, Hardisty-Hughes R, Brown SD: Mouse models as a tool to unravel the genetic basis for human otitis media. Brain Res 2006, 1091:9–15
17. Cunsolo E, Marchioni D, Leo G, Incorvaia C, Presutti L: Functional anatomy of the eustachian tube. Int J Immunopathol Pharmacol 2010, 23(1 Suppl):4–7
18. Silveira Netto LF, da Costa SS, Sleifer P, Braga ME: The impact of chronic suppurative otitis media on children's and teenagers' hearing. Int J Pediatr Otorhinolaryngol 2009, 73:1751–1756
19. Pagella F, Colombo A, Gatti O, Giourgos G, Matti E: Rhinosinusitis and otitis media: the link with adenoids. Int J Immunopathol Pharmacol 2010, 23(1 Suppl):38–40
20. Marseglia GL, Caimmi D, Pagella F, Matti E, Labó E, Licari A, Salpietro A, Pelizzo G, Castellazzi AM: Adenoids during childhood: the facts. Int J Immunopathol Pharmacol 2011, 24(4 Suppl):1–5
21. Syggelou A, Fanos V, Iacovidou N: Acute otitis media in neonatal life: a review. J Chemother 2011, 23:123–126
22. Reiss M, Reiss G: Die chronische eitrige Otitis: Ursachen, Diagnostik und Therapie [Suppurative chronic otitis media: etiology, diagnosis and therapy]. German. Med Monatsschr Pharm 2010, 33:11–16; quiz 17–18
23. Corbeel L: What is new in otitis media? Eur J Pediatr 2007, 166:511–519
24. Qin Z, Wood M, Rosowski JJ: Measurement of conductive hearing loss in mice. Hear Res 2010, 263:93–103
25. Post JC: Genetics of otitis media. Adv Otorhinolaryngol 2011, 70:135–140
26. Preciado D, Kuo E, Ashktorab S, Manes P, Rose M: Cigarette smoke activates NFkappaB-mediated Tnf-alpha release from mouse middle ear cells. Laryngoscope 2010, 120:2508–2515
27. Cooter MS, Eisma RJ, Burleson JA, Leonard G, Lafreniere D, Kreutzer DL: Transforming growth factor-beta expression in otitis media with effusion. Laryngoscope 1998, 108:1066–1070
28. Shi Y, Massagué J: Mechanisms of TGF-beta signaling from cell membrane to the nucleus. Cell 2003, 113:685–700

29. Massagué J, Chen YG: Controlling TGF-beta signaling. Genes Dev 2000, 14:627–644
30. Kouskoura T, Fragou N, Alexiou M, John N, Sommer L, Graf D, Katsaros C, Mitsiadis TA: The genetic basis of craniofacial and dental abnormalities. Schweiz Monatsschr Zahnmed 2011, 121:636–646
31. Maraldi NM, Capanni C, Cenni V, Fini M, Lattanzi G: Laminopathies and lamin-associated signaling pathways. J Cell Biochem 2011, 112:979–992
32. Kondé E, Bourgeois B, Tellier-Lebegue C, Wu W, Pérez J, Caputo S, Attanda W, Gasparini S, Charbonnier JB, Gilquin B, Worman HJ, Zinn-Justin S: Structural analysis of the Smad2-MAN1 interaction that regulates transforming growth factor-beta signaling at the inner nuclear membrane. Biochemistry 2010, 49:8020–8032
33. Burhans WC, Heintz NH: The cell cycle is a redox cycle: linking phase-specific targets to cell fate. Free Radic Biol Med 2009, 47:1282–1293
34. Bengtsson L: What MAN1 does to the Smads. TGFbeta/BMP signaling and the nuclear envelope. FEBS J 2007, 274:1374–1382
35. Van Berlo JH, Voncken JW, Kubben N, Broers JL, Duisters R, van Leeuwen RE, Crijns HJ, Ramaekers FC, Hutchison CJ, Pinto YM: A-type lamins are essential for TGF-beta1 induced PP2A to dephosphorylate transcription factors. Hum Mol Genet 2005, 14: 2839–2849
36. Ohnishi M, Razzaque MS: Dietary and genetic evidence for phosphate toxicity accelerating mammalian aging. FASEB J 2010, 24: 3562–3571
37. Brancaccio D, Tetta C, Gallieni M, Panichi V: Inflammation, CRP, calcium overload and a high calcium-phosphate product: a "liaison dangereuse". Nephrol Dial Transplant 2002, 17:201–203
38. Mosser DM, Edwards JP: Exploring the full spectrum of macrophage activation [Erratum appeared in Nat Rev Immunol 2010, 10:460]. Nat Rev Immunol 2008, 8:958–969
39. Leendertse M, Willems RJ, Giebelen IA, Roelofs JJ, van Rooijen N, Bonten MJ, van der Poll T: Peritoneal macrophages are important for the early containment of Enterococcus faecium peritonitis in mice. Innate Immun 2009, 15:3–12
40. Locksley RM, Killeen N, Lenardo MJ: The TNF and TNF receptor superfamilies: integrating mammalian biology. Cell 2001, 104:487–501
41. Annes JP, Munger JS, Rifkin DB: Making sense of latent TGFbeta activation. J Cell Sci 2003, 116:217–224
42. Taylor AW: Review of the activation of TGF-beta in immunity. J Leukoc Biol 2009, 85:29–33